Basement Relief Inversion: A Comparative Study of the Dual Simplex and a Memetic Algorithm

Arthur A. C. R. Silva, Bruno M. Carvalho, Francisco M. Barboza, Matheus S. Menezes
Federal University of Rio Grande do Norte - Brazil
arthur.romao@ufrn.br, bruno@dimap.ufrn.br, marcio.barboza@ufrn.br, matheus.menezes@ufrn.br

***Abstract*—This paper addresses the inverse problem of reconstructing basement relief from gravity data by comparing two contrasting optimization strategies: a novel linearized approach based on the *Dual-Simplex* (DS) method and a hybrid evolutionary algorithm specifically designed for this problem, namely a *Memetic Algorithm* (MA), which combines global evolutionary operators with Gauss–Newton local refinement. The DS method solves a Linear Programming (LP) formulation based on an L_1-norm data misfit with smoothness regularization, whereas the MA integrates global exploration mechanisms—such as BLX-α crossover, hybrid mutation, and tournament selection—with a weighted local update scheme. Both approaches are applied to synthetic and real 2D datasets: the Isolated Graben model and the Poem Bridge profile. For the synthetic case, characterized by smooth geometry and weak nonlinearity, the DS method achieves higher accuracy, reaching a 1% relative error in 98% of the observations. In contrast, for the more heterogeneous and nonlinear Poem Bridge dataset, the MA demonstrates superior performance in terms of cumulative relative data misfit reduction, achieving a 5% error in approximately 72% of the data, compared to 58% for the DS method. These results indicate that deterministic linearized methods are highly efficient for well-behaved models, whereas evolutionary strategies provide greater robustness in complex, real-world scenarios. Overall, this study highlights the importance of selecting inversion strategies according to the degree of nonlinearity and geological complexity, demonstrating that hybrid metaheuristic approaches can effectively complement classical optimization techniques in geophysical inverse problems.**

***Keywords*—basement relief, inverse problem, Dual-Simplex, Memetic Algorithm, computational Geophysics.**

I. Introduction

The reconstruction of basement relief from gravity data is a classical geophysical inverse problem, widely recognized for its ill-posedness in the Hadamard sense, in which solutions may not exist, may be non-unique, or may exhibit strong sensitivity to measurement noise [1]. Such characteristics require a careful mathematical formulation and robust numerical strategies to produce geologically meaningful models.

Basement relief inversion plays a key role in numerous geophysical applications, including: (i) delineation of sedimentary basin architecture for hydrocarbon exploration [2, 3]; (ii) identification of tectonic domains such as grabens, horsts, and fault-controlled depressions [4, 5]; (iii) mapping of structural discontinuities and lateral density variations in the crust [6, 7]; (iv) support for near-surface engineering and geotechnical investigations [8, 9]; and (v) data-driven approaches using deep learning to estimate 2D and 3D basement geometries directly from gravity fields [10–13]. These diverse applications highlight the importance of developing reliable, accurate, and computationally efficient inversion methods.

In this study, the problem is formulated in two dimensions, with the basement represented by a set of vertically oriented prisms. The basement depth vector $\mathbf{d}$ specifies the geometry, while predicted gravity anomalies $\mathbf{g}_{\text{obs}}$ are obtained by applying a nonlinear forward operator that relates density contrasts to surface measurements. A key modeling feature is that the sensitivity matrix $\mathbf{A}$ is constructed using *unit-height prisms*, which exploits the linear dependence of the gravity response on prism height. As a consequence, the Jacobian remains constant throughout the inversion, considerably reducing computational cost and improving numerical stability.

The combination of nonlinearity, measurement noise, limited spatial coverage, and the presence of outliers in real gravimetric data further underscores the need for regularization to stabilize the inversion [14]. In this work, both the data misfit and the regularization terms are formulated using the L_1 norm. The L_1 norm is well known for its robustness to outliers and non-Gaussian noise, as it is equivalent to assuming a Laplacian error distribution with heavier tails than the Gaussian distribution associated with the L_2 norm [15–17]. Consequently, large residuals are penalized linearly rather than quadratically, preventing isolated corrupted observations from dominating the inversion process. This property is particularly relevant in gravity inversion, where data contamination may arise from acquisition errors, regional–residual separation, terrain corrections, or unmodeled geological heterogeneities [18, 19].

In addition, the use of the L_1 norm in regularization promotes sparsity in the gradient of the model, favoring piecewise-smooth or blocky structures that are more consistent with geological expectations for basement relief and fault-controlled domains [20–22]. Compared with classical L_2 smoothness constraints, L_1-based regularization better preserves sharp interfaces and structural discontinuities, which are fundamental characteristics of tectonic features such as grabens and horsts.

A variety of regularization strategies have been proposed in the literature, including smoothness constraints [18], entropic regularization [19], and Total Variation formulations [20, 21].

Among these, L_1-based approaches have gained increasing attention due to their combined robustness and structural preservation capabilities [15–17].

In parallel, global and hybrid metaheuristic optimization methods have gained traction, particularly in strongly nonlinear scenarios [23–25]. Representative examples include particle swarm optimization [26], ant colony–based algorithms [24], and simulated annealing [27]. These methods are especially attractive because they do not rely on local linearization and are less sensitive to the initial model.

Against this background, the present work compares two complementary inversion strategies:

1) A new deterministic linearized method based on an L_1-norm data misfit combined with L_1-norm smoothness regularization, formulated as a linear programming (LP) problem and solved using the *Dual-Simplex (DS)* algorithm [28–30]. In this new formulation, the robustness of the L_1 norm is directly embedded in the optimization structure, resulting in a stable and computationally efficient approach for large and sparse systems.
2) A *Memetic Algorithm (MA)* that integrates global evolutionary operators (BLX-α crossover, hybrid mutation, and tournament selection) with a local refinement stage based on a weighted Gauss–Newton update [25, 31–33]. The global search uses an L_1 objective function, ensuring robustness to outliers and structural preservation, while the local Gauss–Newton step employs an L_2 formulation for computational efficiency and fast convergence in the vicinity of promising solutions. This hybrid L_1–L_2 strategy combines robustness at the global level with numerical efficiency at the local level.

Both strategies are assessed using synthetic and real 2D datasets—the Isolated Graben Model and the Poem Bridge Model—allowing for a comprehensive evaluation under both controlled and real-world conditions. The comparison focuses on the accuracy of basement-geometry reconstruction and on data-fit quality, as reflected by the behavior of the cumulative relative data-misfit error.

II. Methodology

A. Forward Model

We consider a 2D gravity profile discretized into η adjacent vertical rectangular prisms with fixed lateral width and constant density contrast. The model parameters correspond to the basement depths, represented by the prism thicknesses d_j.

Figure 1 illustrates the forward modeling framework for a 2D sedimentary basin. Subfigure (a) shows the observed gravity anomaly at the surface, while subfigure (b) presents the discretized basement topography, approximated by η adjacent rectangular prisms with varying heights p_j, which are directly related to the parameters d_j. A constant horizontal spacing Δx between observation points is assumed. In the 2D formulation, the gravity anomaly at each observation point is computed using the analytical solution for the vertical component of the gravitational attraction of rectangular prisms. The total anomaly is obtained by superposition of the contributions from all prisms.

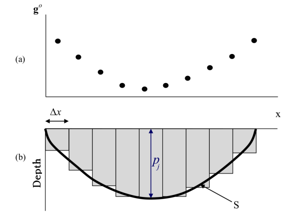

Figure 1. (a) Observed gravity anomaly at the surface; (b) Sedimentary basin model in which the basement topography S is approximated by η juxtaposed 2D rectangular prisms of height p_j. Each prism contributes to the total gravity anomaly at the observation points. Source: [9]

The gravity anomaly at the i-th of μ observation points is given by:

$$\mathbf{F}_i(\mathbf{d}) = \sum_{j=1}^{\eta} f(\rho_j, d_j, r_{ij}), \tag{1}$$

where ρ_j is the density contrast of prism j, and r_{ij} describes the geometric relationship between the i-th observation point and the j-th prism, including their relative horizontal and vertical distances.

The kernel function f corresponds to the classical analytical expression for the vertical component of the gravitational attraction of a 2D rectangular body [2].

B. Sensitivity Matrix and Linearization

The Jacobian matrix $\mathbf{J}(\mathbf{d}) = \partial \mathbf{F}/\partial \mathbf{d} \in \mathbb{R}^{\mu \times \eta}$ quantifies the sensitivity of the data to the model parameters.

Sensitivity Matrix for Linear Inversion: For a linear approximation, the model is represented by unit-density prisms, yielding $\mathbf{g} \approx \mathbf{A}\mathbf{d}$. The sensitivity matrix $\mathbf{A}$ is precomputed by evaluating the forward response for each prism with unit thickness:

$$A_{ij} = F(\mathbf{e}_j)_i, \tag{2}$$

leading to a constant Jacobian: $\mathbf{J}_\tau \equiv \mathbf{A}$.

Finite-Difference Jacobian for Gauss–Newton: For nonlinear refinement, a numerical Jacobian is computed via finite differences. For a current model $\mathbf{d}_0$:

$$\mathbf{J}_{:,j} \approx \frac{\mathbf{F}(\mathbf{d}_0 + \gamma\delta_j\mathbf{e}_j) - \mathbf{F}(\mathbf{d}_0)}{\gamma\delta_j}, \tag{3}$$

where $\gamma = 1$ and $\delta_j = 10^{-3}\max\{|d_{0,j}|, 10^{-5}\}$. The Jacobian is stored in sparse format.

C. Objective Function

We employ an L_1 norm for robustness against outliers, combined with Total Variation regularization [20]:

$$\mathcal{J}(\mathbf{d}) = \|\mathbf{g}_{\text{obs}} - \mathbf{F}(\mathbf{d})\|_1 + \lambda\|\mathbf{D}\mathbf{d}\|_1, \tag{4}$$

where the first term represents the data misfit between the observed data ($\mathbf{g}_{\text{obs}}$) and the data calculated by the forward model ($\mathbf{F}(\mathbf{d})$, as defined in 1), and the second term corresponds to the regularization; $\lambda > 0$ is the regularization parameter, and $\mathbf{D}$ is the first-order finite-difference matrix.

D. Linearized L_1 Inversion with DS

Starting from an estimate $\mathbf{d}_\tau$, the forward operator is linearized:

$$\mathbf{F}(\mathbf{d}) \approx \mathbf{F}(\mathbf{d}_\tau) + \mathbf{A}(\mathbf{d} - \mathbf{d}_\tau). \quad (5)$$

With the residual $\Delta\mathbf{r}_\tau = \mathbf{g}_{obs} - \mathbf{F}(\mathbf{d}_\tau)$ and model increment $\Delta\mathbf{d} = \mathbf{d} - \mathbf{d}_\tau$, we solve the linearized subproblem:

$$\min_{\Delta\mathbf{d}} \|\mathbf{A}\Delta\mathbf{d} - \Delta\mathbf{r}_\tau\|_1 + \lambda\|\mathbf{D}\Delta\mathbf{d}\|_1. \quad (6)$$

To solve this L_1 problem, we introduce auxiliary variables $\mathbf{u} \geq 0$ and reformulate it as a Linear Programming (LP) problem:

$$\min_{\mathbf{x}} \quad \mathbf{f}^\mathsf{T}\mathbf{x}, \quad \text{where } \mathbf{x} = [\Delta\mathbf{d}; \mathbf{u}], \quad (7)$$

$$\text{subject to} \quad \mathbf{A}_{\text{ineq}}\mathbf{x} \leq \mathbf{b}_{\text{ineq}}, \ \mathbf{u} \geq \mathbf{0}. \quad (8)$$

The matrices are defined as:

$$\mathbf{f} = [\mathbf{0}; \mathbf{1}], \quad \mathbf{A}_{\text{aug}} = [\mathbf{A}; \sqrt{\lambda}\mathbf{D}], \quad \mathbf{b}_{\text{aug}} = [\Delta\mathbf{r}_\tau; \mathbf{0}], \quad (9)$$

$$\mathbf{A}_{\text{ineq}} = \begin{bmatrix} \mathbf{A}_{\text{aug}} & -\mathbf{I} \\ -\mathbf{A}_{\text{aug}} & -\mathbf{I} \end{bmatrix}, \quad \mathbf{b}_{\text{ineq}} = \begin{bmatrix} \mathbf{b}_{\text{aug}} \\ -\mathbf{b}_{\text{aug}} \end{bmatrix}. \quad (10)$$

This bound-constrained LP is solved using the *DS* algorithm for its efficiency with sparse problems. The complete iterative procedure is detailed in Algorithm 1.

Algorithm 1: Linearized L_1 Inversion (*DS*)

Require: Initial model $\mathbf{d}_0$, observed data $\mathbf{g}_{obs}$, tolerance ϵ, max iterations Γ, max LP iterations Γ_ω, regularization λ
Ensure: Estimated model $\mathbf{d}^*$

```
Precompute sensitivity matrix A using unit-height prisms
Construct smoothing operator D and augmented matrix A_aug
for τ = 0 to Γ − 1 do
    Compute predicted data: g_τ = A d_τ
    Compute residual: Δr_τ = g_obs − g_τ
    Form augmented RHS: b_aug = [Δr_τ^T, 0^T]^T
    Build LP matrices f, A_ineq, b_ineq
    Solve LP via DS (max Γ_ω iterations) to obtain Δd
    Update model: d_{τ+1} = d_τ + Δd
    if ‖Δd‖/‖d_τ‖ < ϵ then
        break
    end if
end for
d* = d_{τ+1}
```

E. MA with Gauss–Newton Local Search

The second strategy is a *MA* combining global evolutionary exploration with local Gauss–Newton refinement.

Initialization and Fitness: An initial population of Ω individuals is generated by sampling each parameter uniformly within the inversion bounds $[\mathbf{d}_{\min}, \mathbf{d}_{\max}]$. Each candidate model $\mathbf{d}_i$ is evaluated using the objective function $\mathcal{J}(\mathbf{d}_i)$ (as defined in 4).

BLX-α Crossover with Adaptive Parameter: A fraction P_c of the population undergoes BLX-α crossover. For parents $\mathbf{p}^{(1)}$ and $\mathbf{p}^{(2)}$, the crossover interval for parameter j is:

$$C_j = [\min(p_j^{(1)}, p_j^{(2)}) - \alpha\Delta_j, \ \max(p_j^{(1)}, p_j^{(2)}) + \alpha\Delta_j],$$

where $\Delta_j = |p_j^{(1)} - p_j^{(2)}|$. The parameter α decays linearly over generations to transition from exploration to exploitation: $\alpha_\tau = \alpha_{\text{BLX}}(1 - 0.5\tau/\Gamma)$.

Hybrid Adaptive Mutation: Each offspring undergoes mutation with probability ζ, using a hybrid Gaussian/uniform scheme. The mutation amplitude σ_τ decreases linearly from σ_{init} to σ_{final} over the generations.

Local Gauss–Newton Refinement (25% of Offspring): To accelerate convergence, 25% of the offspring (as selected empirically) are randomly chosen for refinement using the Weighted Gauss–Newton (WGN) method. For a candidate $\mathbf{d}_0$:

1) Compute the Jacobian $\mathbf{J}$ via finite differences.
2) Compute the residual $\Delta\mathbf{g} = \mathbf{g}_{obs} - \mathbf{F}(\mathbf{d}_0)$.
3) Solve the regularized normal equations: $(\mathbf{J}^\mathsf{T}\mathbf{J} + \lambda\mathbf{D}^\mathsf{T}\mathbf{D})\Delta\mathbf{d} = \mathbf{J}^\mathsf{T}\Delta\mathbf{g}$.
4) Update the model: $\mathbf{d}_0 \leftarrow \mathbf{d}_0 + \beta\Delta\mathbf{d}$, where $\beta \in \mathcal{H} = \{0.5, 0.8, 1.0, 1.2, 1.5\}$.
5) Accept the refined model only if $\mathcal{J}$ improves.

Tournament Selection and Population Update: Parents and offspring are merged into a common pool. The next generation is formed via deterministic tournament selection: for each slot, ι candidates are sampled, and the one with the lowest $\mathcal{J}$ is selected.

Stopping Criteria: The algorithm runs for up to Γ generations. It stops early if the relative improvement of the best fitness $\mathcal{B}_\tau < \xi$ (with $\xi = 10^{-4}$) for κ consecutive generations, where:

$$\mathcal{B}_\tau = \frac{|\mathcal{J}_{\text{best}}^{(\tau)} - \mathcal{J}_{\text{best}}^{(\tau-1)}|}{\max(|\mathcal{J}_{\text{best}}^{(\tau-1)}|, \varepsilon)}, \quad \varepsilon = 10^{-16}.$$

The complete procedure is summarized in Algorithm 2.

III. Results and Discussion

The experiments were conducted under two distinct scenarios: (i) a two-dimensional (2D) synthetic geological model representing an isolated graben basin, and (ii) a real-world application at the Poem Bridge site. In both scenarios, the control parameters of the inversion algorithms were tuned using the *irace* library [34], which provides an automated and statistically principled framework for parameter configuration. For each model and method considered in this study, the best-performing configuration was selected based on ten independent runs, using the lowest objective-function cost as the selection criterion after *irace* tuning. Due to hardware limitations, only a subset of parameters was optimized. For the *DS* method, the maximum number of iterations Γ and the regularization parameter λ were tuned. For the *MA*, the tuned parameters included the population size Ω, the number of generations Γ, the mutation probability ζ, the gene mutation probability ς, and the regularization parameter λ. All

Algorithm 2: *MA* with Gauss–Newton Local Search

Require: Objective $\mathcal{J}$, bounds, pop. size Ω, max gen. Γ, crossover rate P_c, mutation rates (ζ, ς), α_{BLX}, σ_{init}, σ_{final}, tournament size ι, reg. param λ, stopping tol. ξ, κ
Ensure: Best model $\mathbf{d}^*$ and fitness $\mathcal{J}(\mathbf{d}^*)$
Initialize population $\{\mathbf{d}_i\}_{i=1}^{\Omega}$ uniformly within bounds
Evaluate fitness $\mathcal{J}(\mathbf{d}_i)$ for all individuals
Store initial best model and fitness
for $\tau = 1$ to Γ **do**
  Update adaptive parameters: α_τ, σ_τ
  Select parents, apply BLX-α_τ crossover
  Apply hybrid mutation (probability ζ at individual level, ς at gene level)
  Select 25% of offspring for WGN refinement with step size from $\mathcal{H}$; accept only if fitness improves
  Merge parents and offspring into a unified pool
  Recompute fitness values as required
  Form next population via tournament selection (size ι)
  Update best model and fitness history
  if $\mathcal{B}_\tau < \xi$ for κ consecutive iterations **then**
    break
  end if
end for
return best model and corresponding fitness

algorithms were implemented and executed in the MATLAB environment [35].

A. Isolated Graben

The isolated graben model represents a structural depression formed by normal faults in extensional tectonic settings, where crustal stretching causes a central block to subside relative to its flanks, creating a typical V-shaped geometry. Over time, these basins accumulate thick sedimentary sequences whose wedge-shaped structures are controlled by fault activity and subsidence. In this synthetic case, basement variations generate a non-uniform interface with the sedimentary cover, producing measurable gravity anomalies due to density contrasts. Because isolated grabens are common hydrocarbon traps and widely used as benchmark models in inversion studies, this configuration provides a reliable and controlled framework for evaluating algorithm performance [2, 3, 36].

The model was discretized into $\eta = 60$ vertical prisms with constant width $\Delta x = 1$ km and a uniform density contrast of $\rho = -0.25$ g/cm^3. A total of $\mu = 60$ synthetic gravity observations were generated.

For the isolated graben experiment, the *DS* algorithm was configured with a tolerance $\epsilon = 10^{-5}$, a maximum of $\Gamma = 15$ outer iterations, and up to $\Gamma_\omega = 10,000$ internal iterations. The regularization parameter was set to $\lambda = 25$.

The *MA* employed a population size of $\Omega = 100$ individuals over $\Gamma = 110$ generations. Each individual was refined through a local search procedure with $\Gamma_\omega = 10$ iterations. The mutation probability was set to $\zeta = 0.2$, with a gene mutation probability of $\varsigma = 0.1$. A crossover rate of $P_c = 0.75$ was adopted using the BLX-α operator with $\alpha_{\text{BLX}} = 0.3$. The mutation scale decreased linearly from $\sigma_{\text{init}} = 0.1$ to $\sigma_{\text{final}} = 0.01$. Tournament selection was applied with a tournament size of $\iota = 3$. The stopping criteria included a tolerance $\xi = 10^{-5}$ and a stagnation limit of $\kappa = 20$ generations. The regularization parameter was also set to $\lambda = 25$.

Figure 2 presents the adjusted isolated graben model and its data, along with the results obtained using *DS* and *MA*.

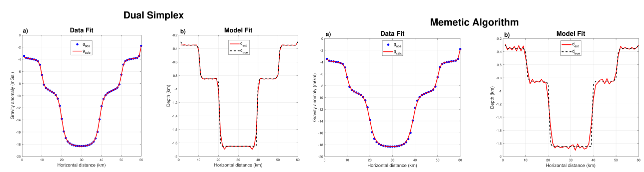

Figure 2. Model fit (a) and data fit (b) obtained using the *DS* algorithm (left) and the *MA* algorithm (right).

Both algorithms provided good fits to the synthetic gravity data; however, their estimated basement geometries differ significantly. The *DS* method reconstructed a geometry that closely matches the true graben structure, preserving both the amplitude and curvature imposed by the bounding faults. In contrast, the *MA* produced a somewhat unstable interface, a behavior commonly observed due to the presence of noise and its exploratory nature, which may drive convergence toward spurious solutions. This may lead to convergence toward the optimum of a perturbed objective function, as if the true search space were obscured and the ideal minimum hidden by noise.

Figure 3 shows the cumulative relative data misfit error for both methods [37]. The *DS* algorithm achieved superior accuracy, reaching a relative error below 1% for approximately 98% of the gravity observations. In comparison, the *MA* achieved the same accuracy threshold for only 78% of the data. These results highlight the effectiveness of local deterministic optimization in synthetic scenarios characterized by smooth and near-linear geometries.

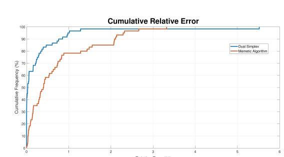

Figure 3. Cumulative relative data misfit error for the *DS* and *MA*.

B. Poem Bridge

Gravimetric inversion techniques have previously been applied to real data acquired at the Poem Bridge, located on the Belém campus of the Federal University of Pará (UFPA), as reported by Lima [38] and Santos et al. [9]. Figure 4 shows, on the left, a photograph of the site, highlighting the W–E profile, the topographic gradients g_1 and g_2, and the reinforced concrete piles A and B. These piles act as localized high-density sources, generating strong gravity anomalies relative to the surrounding unconsolidated soil.

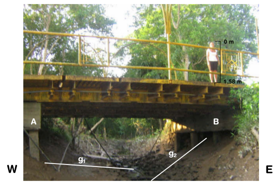

Figure 4. Photograph of the Poem Bridge showing the W–E gravimetric profile. The western side exhibits a more abrupt discontinuity than the eastern side. Source: [39].

For this real-data experiment, a density contrast of $\rho = -2.3$ g/cm^3 was assumed. The gravity profile extends over 22.5 m and was discretized into $\eta = 45$ vertical prisms with width $\Delta x = 0.5$ m, resulting in $\mu = 40$ gravity observations. Based on previous studies, the maximum depth to the basement was visually estimated at approximately 3.3 m [39].

The initial depth estimate d_0 was computed using the Bouguer slab approximation [40]. For the Poem Bridge dataset, both algorithms were configured with the same regularization parameter $\lambda = 0.02$ to account for the shallow and highly heterogeneous subsurface conditions.

The *DS* algorithm was configured with a tolerance $\epsilon = 10^{-5}$, a maximum of $\Gamma = 11$ iterations, and $\Gamma_\omega = 10,000$ internal iterations.

The *MA* employed a population of $\Omega = 130$ individuals evolved over $\Gamma = 114$ generations, with a local search phase of $\Gamma_\omega = 10$ iterations. The mutation probability and gene mutation probability were set to $\zeta = 0.23$ and $\varsigma = 0.12$, respectively. A crossover rate of $P_c = 0.75$ was adopted using the BLX-α operator ($\alpha_{\text{BLX}} = 0.3$). The mutation scale decreased from $\sigma_{\text{init}} = 0.1$ to $\sigma_{\text{final}} = 0.01$. Tournament selection used a size of $\iota = 3$, with convergence controlled by a tolerance $\xi = 10^{-5}$ and a stagnation limit of $\kappa = 20$ generations.

Figure 5 presents the fit between the observed and calculated data (a), along with the corresponding model reconstructions obtained using *DS* (left) and *MA* (right) (b), in addition to the Bouguer-based initial approximation. Although both methods reproduce the general trend of the observed gravity anomaly, their estimated geometries differ significantly. This discrepancy reflects the limitations of the Bouguer-based initialization, which provides only a crude approximation and fails to capture the true subsurface complexity, particularly in the presence of strong density contrasts such as those associated with the concrete piles. Figure 6 shows the cumulative relative

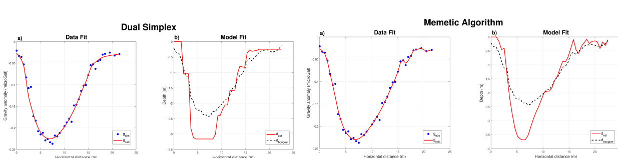

Figure 5. (a) Data fit and (b) model reconstruction obtained using the *DS* (left) and *MA* (right) methods.

data misfit error for both inversion techniques [37]. In contrast to the synthetic experiment, the *MA* outperformed the *DS* method on the real dataset. The *MA* achieved a relative error below 5% for approximately 72% of the observations, whereas the *DS* method reached the same threshold for only 58%. This result highlights the advantage of global search strategies in real-world problems that violate local linearity assumptions, where the subsurface exhibits strong heterogeneity and highly nonlinear behavior.

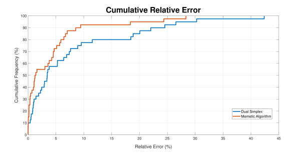

Figure 6. Cumulative relative data misfit error for the *DS* and *MA* methods applied to the Poem Bridge dataset.

IV. Conclusion

This study evaluated the performance of two inversion strategies—*DS* and *MA*—applied to both synthetic and real gravimetric datasets. In the synthetic isolated graben model, the subsurface geometry was simple, the forward modeling was fully known, and the same assumptions used to generate the data were also adopted in the inversion. Under these conditions, the linearized *DS* method demonstrated superior performance. The consistency between the true model and the inversion model, combined with the well-behaved topology of the objective function, favored linearization, enabling rapid convergence and high accuracy.

In contrast, the real Poem Bridge dataset presented a markedly different scenario. Real-world problems introduce heterogeneity, structural discontinuities, and a complex, data-dependent objective-function topology. Such complexity alters the landscape of the inversion problem for each dataset. In these cases, linearization may discard crucial information during the approximation process, leading to suboptimal convergence. The *MA*, by incorporating a global evolutionary search, demonstrated a more robust ability to explore the parameter space, escape local minima, and adapt to the nonlinear nature of the true density distribution. Its superior data misfit reduction in the real case is therefore attributed to its ability to preserve information that purely local methods tend to lose.

Beyond the comparative evaluation of inversion strategies, this work introduces several methodological contributions. First, both inversion approaches are formulated within an L_1-norm framework for data misfit and regularization. This choice provides robustness against outliers and non-Gaussian noise by implicitly assuming a heavy-tailed (Laplacian) error distribution, while also promoting sparsity in the model gradients and preserving sharp geological discontinuities. As a result, the inversion becomes more resilient to contaminated measurements and more consistent with the blocky nature of tectonic basement structures.

Second, we propose a novel linearization approach for basement–relief gravity inversion based on constructing the sensitivity matrix $\mathbf{A}$ using unit-height prisms. This formulation exploits the intrinsic linearity of the forward response with respect to prism height and allows the Jacobian to remain constant across iterations. Despite its simplicity and computational advantages, this strategy remains largely unexplored in the existing literature. By decoupling geometric effects from density scaling and eliminating the need to recompute derivatives at each iteration, this approach provides an efficient and stable foundation for linear L_1 inversion, particularly relevant for large-scale or computationally constrained applications.

Third, in the *MA*, we demonstrate the effectiveness of combining an L_1-based global objective function with an L_2-based local Gauss–Newton refinement. The L_1 norm ensures robustness and structural preservation during the evolutionary search, while the L_2 norm in the local step provides fast convergence and numerical stability near promising solutions. This hybrid L_1–L_2 strategy represents a practical compromise between robustness and efficiency and highlights the complementary nature of different norms in inverse problem optimization.

Finally, for this specific problem, linearized local inversion methods are efficient and highly effective for simple or well-behaved models, whereas evolutionary and hybrid algorithms become essential when dealing with real-world datasets characterized by strong nonlinearity, heterogeneous structures, outliers, and complex objective-function topologies.

Future work may include evaluating alternative local-search strategies within the *MA* framework, exploring different hybrid norm combinations, and investigating new ways to construct sensitivity matrices that further reduce information loss during inversion. Ultimately, the *DS* and *MA* approaches should be viewed as complementary tools, and the choice between them should be guided by the geological complexity of the target area and the desired balance between computational cost, robustness, and interpretational accuracy.

ACKNOWLEDGEMENTS

This study was financed in part by the Coordenação de Aperfeiçoamento de Pessoal de Nível Superior - Brasil (CAPES) - Finance Code 001.

REFERENCES

[1] J. Hadamard, "Sur les problèmes aux dérivées partielles et leur signification physique," 1902, Princeton Univ. Bull., pp. 49–52.

[2] W. M. Telford *et al.*, *Appl. Geophys.* Cambridge Univ. Press, 1990.

[3] P. Kearey, M. Brooks, and I. Hill, *An Introduction to Geophysical Exploration*. John Wiley & Sons, 2013.

[4] O. Pamukçu, A. S. Pamukçu, and Z. Akçığ, "Gravity data inversion for the basement relief delineation through global optimization: A case study from the aegean graben system, western anatolia, turkey," *Geophys. J. Int.*, vol. 224, no. 2, pp. 923–940, 2020.

[5] Y. L. Ekinci, Ç. Balkaya, G. Göktürkler, and H. Ai, "3-D gravity inversion for the basement relief reconstruction through modified success-history-based adaptive differential evolution," *Geophys. J. Int.*, vol. 235, no. 1, pp. 377–400, 2023.

[6] V. C. F. Barbosa, J. B. Silva, and W. E. Medeiros, "Gravity inversion of basement relief using approximate equality constraints on depths," *Geophysics*, vol. 62, no. 6, pp. 1745–1757, 1997.

[7] D. F. Santos *et al.*, "Efficient gravity inversion of discontinuous basement relief," *Geophys.*, vol. 80, no. 4, pp. G95–G106, 2015.

[8] J. B. Silva *et al.*, "Fast gravity inversion of basement relief," *Geophys.*, vol. 79, no. 5, pp. G79–G91, 2014.

[9] R. D. C. S. d. Santos *et al.*, "Inversão gravimétrica rápida do relevo do embasamento aplicando o funcional da variação total," Master's thesis, UFPA, Brazil, 2013.

[10] S. He *et al.*, "Recovering 3D basement relief using gravity data through convolutional neural networks," *J. Geophys. Res.: Solid Earth*, vol. 126, no. 10, p. e2021JB022611, 2021.

[11] C. Dubey *et al.*, "Basement relief of sedimentary basin using gravity data from deep neural network approach," *J Geol Geophys*, vol. 12, p. 1066, 2023.

[12] Y. Zhang *et al.*, "3D basement relief and density inversion based on efficientnetv2 deep learning network," *IEEE Trans. Geosci. Rem. Sens.*, vol. 62, pp. 1–15, 2024.

[13] H. Cai *et al.*, "Effective gravity inversion of basement relief with unfixed density contrast using deep learning," *Comput. & Geosci.*, vol. 196, p. 105832, 2025.

[14] H. W. Engl, M. Hanke, and A. Neubauer, *Regularization of Inverse Problems*. Springer Sci. & Bus. Media, 1996, vol. 375.

[15] P. J. Huber, *Robust Statistics*. John Wiley & Sons, 1981.

[16] T. F. Chan and J. Shen, "Image processing and analysis: Variational, PDE, wavelet, and stochastic methods," *SIAM*, 2005.

[17] S. Boyd *et al.*, "Distributed optimization and statistical learning via the alternating direction method of multipliers," *Found. Trends in Mach. Learn.*, vol. 3, no. 1, pp. 1–122, 2011.

[18] V. C. F. Barbosa and J. B. Silva, "Generalized compact gravity inversion," *Geophys.*, vol. 59, no. 1, pp. 57–68, 1994.

[19] J. B. Silva *et al.*, "Gravity inversion of 2D basement relief using entropic regularization," *Geophysics*, vol. 75, no. 3, pp. I29–I35, 2010.

[20] C. M. Martins *et al.*, "Total variation regularization for depth-to-basement estimate: Part 1 — Mathematical details and applications," *Geophys.*, vol. 76, no. 1, pp. I1–I12, 2011.

[21] W. A. Lima *et al.*, "Total variation regularization for depth-to-basement estimate: Part 2 — Physicogeologic meaning and comparisons with previous inversion methods," *Geophys.*, vol. 76, no. 1, pp. I13–I20, 2011.

[22] L. I. Rudin *et al.*, "Nonlinear total variation based noise removal algorithms," *Physica D*, vol. 60, no. 1-4, pp. 259–268, 1992.

[23] J. Pallero *et al.*, "Gravity inversion and uncertainty assessment of basement relief via particle swarm optimization," *J. Appl. Geophys.*, vol. 116, pp. 180–191, 2015.

[24] A. Joolaei *et al.*, "Basement relief modeling by gravity inversion via ant colony algorithm," *Iran. J. of Geophys.*, vol. 14, no. 1, pp. 39–54, 2020.

[25] S. Carbas *et al.*, "Nature-inspired metaheuristic algorithms for engineering optimization applications," *Appl. Sci.*, vol. 9, no. 24, p. 5528, 2019.

[26] J. Pallero *et al.*, "3D gravity inversion and uncertainty assessment of basement relief via particle swarm optimization," *J. Appl. Geophys.*, vol. 139, pp. 338–350, 2017.

[27] O. Mojica and A. Bassrei, "Application of the generalized simulated annealing algorithm to the solution of 2D gravity inversion of basement relief," in *3rd Latin Am. Geosci. Stud. Con.*, no. 1, 2015, pp. 1–3.

[28] G. B. Dantzig, *Linear Programming and Extensions*. Princeton Univ. Press, 1963.

[29] P. E. Gill *et al.*, *Practical Optimization*. Academ. Press, 1981.

[30] W. Murray, M. H. Wright, and P. E. Gill, *Practical Optimization*. SIAM-Soc. Ind. and Appl. Math., 2019.

[31] M. K. Sen and P. L. Stoffa, *Global Optimization Methods in Geophysical Inversion*. Cambridge Univ. Press, 2013.

[32] F. Neri and C. Cotta, "Memetic algorithms and memetic computing optimization: A literature review," *Swarm Evolut. Comput.*, vol. 2, pp. 1–14, 2012.

[33] P. Moscato *et al.*, "Memetic algorithms," in *New Optimization Techniques in Engineering*. Springer, 2004, pp. 53–85.

[34] M. López-Ibáñez *et al.*, "The irace package: Iterated racing for automatic algorithm configuration," *Operat. Res. Persp.*, vol. 3, pp. 43–58, 2016.

[35] The MathWorks, Inc., *MATLAB R2018b*, The MathWorks, Inc., Natick, MA, USA, 2018, version 9.5 (R2018b).

[36] R. J. Blakely, *Potential Theory in Gravity & Magnetic Applications*. Cambridge, UK: Cambridge Univers. Press, 1995.

[37] W. L. Martinez and A. R. Martinez, *Computational statistics handbook with MATLAB*. Chapman and Hall/CRC, 2001.

[38] W. A. Lima, "Inversão gravimétrica do relevo de bacias extencionais através da variação total," Master's thesis, PPgG, UFPA, 2009.

[39] J. B. C. Silva *et al.*, "Inversão gravimétrica do relevo do embasamento usando regularização entrópica," in *10th Int. Congr. Brazilian Geophys. Soc. & EXPOGEF 2007, Brazil*. SEG, 2007, pp. 698–703.

[40] M. Bott, "The use of rapid digital computing methods for direct gravity interpretation of sedimentary basins," *Geophys. J. Int.*, vol. 3, no. 1, pp. 63–67, 1960.